Superdiatomics and Picosprings: Cage−Cage Vibrations in $C_{120}O$, $C_{120}O_2$, and in Three Isomers of $C_{130}O$

Hans-Jürgen Eisler, Frank H. Hennrich, Eva Werner, Andreas Hertwig, Carsten Stoermer, and Manfred M. Kappes*

Institut für Physikalische Chemie, Universität Karlsruhe, D-76128 Karlsruhe, Germany

Received: January 22, 1998

The title compounds comprising furanoid- ($C_{120}O$, $C_{130}O$) or bisfuranoid-linked ($C_{120}O_2$) fullerene cages were prepared from $C_{60}O$ and C_{60}/C_{70}. For $C_{130}O$, three isomers were isolated. Following HPLC separation all substances were characterized as (microcrystalline) solids by Raman spectroscopy. Measurements, which in the case of $C_{120}O$ and $C_{120}O_2$ commenced at Stokes shifts greater than 15 cm^{-1}, were interpreted in terms of semiempirical calculations (PM3) both of ground-state energetics as well as of vibrational frequencies. Good agreement between (harmonic) vibrational frequency predictions and Raman spectra was obtained. A comprehensive discussion of low-frequency cage−cage vibrations in fullerene dimers and related compounds is attempted on this basis.

1. Introduction

Connecting fullerene cages has been of interest since the dual observations of fullerene coalescence[1] and photopolymerization[2] upon laser irradiation of C_{60} thin films. Further impetus for such studies has been provided by the observation of pressure-induced polymerization[3] as well as by the spectroscopic and crystallographic inference of fullerene oligomers in various MC_{60} phases (M = alkali).[4] There now exist numerous (planned) synthetic approaches for covalently linking fullerenes while maintaining the essential structural integrity of the individual carbon cage units.[5] Such syntheses have generally been restricted to the most abundant fullerene C_{60}, although they should generally also be applicable to higher fullerenes.

The shortest fullerene links result from cycloadditions connecting just the cages themselves. A 2 + 2 cycloaddition of two C_{60} units gives rise to a dimer bound by two C−C links that together with the cages form a 4-fold ring. The corresponding C_{120} has recently been prepared by KCN-catalyzed mechanochemistry.[6] It is now confirmed[3,4] that 2 + 2 cycloaddition is also the basis of C_{60} pressure- and photopolymerization leading to $(C_{60})_x$ oligomer distributions in the respective solids.[2]

Slightly more complicated are links involving oxygen atoms. A furanoid ring-bridged dimer $C_{120}O$ is known[7,8] as is the tetralinked bis(furanoid) ring-bridged species $C_{120}O_2$.[9] As for C_{120}, $C_{120}O$ connects between double (6,6) bonds of the original cages. In $C_{120}O_2$ the links comprise two furanoid rings sharing C−C interconnects with a central 4-fold ring. Here, in contrast to $C_{120}O$, the four-ring is thought to connect between single (6,5) bonds of the original C_{60}'s. In all dimers the consequence of linkage is a weakening/relaxation of cage bonds adjacent to bridging atoms.

After early mass spectroscopic work established that odd-numbered dimer-related species can be formed by way of fullerene epoxides,[10,11] it has proven possible to isolate C_{119}.[12] This "peanut"-shaped species can be obtained by thermal decomposition of $C_{120}O_x$ ($x < 3$). $C_{120}O$, $C_{120}O_2$, and C_{119} all appear to be intermediates in the oxidative degradation of C_{60}. From ^{13}C NMR measurements, C_{119} is thought to consist of two partially opened cages connected by three sp^3 carbons and two seven-membered rings. Consequently, although it retains a high degree of topological analogy to the title dimers, the structural integrity of the individual cages is no longer maintained in C_{119}.

Stimulated by early speculations that the C_{60} photopolymer contains 2 + 2 cycloadducts,[2] various theoretical methods have been applied to describe the energetics and vibrational properties of C_{120} as well as related fullerene dimers.[13−16] Such treatments have predicted that these molecules comprising large (and heavy) "monomer" units with high structural rigidity connected by two or more comparatively weak (and short) bonds should have unique vibrational properties.[13,14,16] Specifically, the six additional vibrational modes (relative to free monomers) are expected to be low frequency and only weakly coupled to (higher frequency) intracage vibrations. One of these six vibrations, a symmetric cage−cage stretch, has been invoked to explain the 118 cm^{-1} Raman band observed in polymerized C_{60}.[2,13] Intense low-frequency features recently observed near 100 cm^{-1} in Raman measurements of C_{120}, $C_{120}O$, and $C_{120}O_2$ solids have been similarly attributed to diatomic-like symmetric stretch vibrations.[17] For C_{120}, two other weaker Raman features also observed at 127 and 139 cm^{-1} have been assigned to cage−cage torsional modes.

Here, we present data on various fullerene dimers including several new substances in an attempt to provide a comprehensive discussion of the theoretical and experimental aspects of cage−cage vibrations in this compound class. Specifically, Raman spectroscopy (extending in some cases to 15 cm^{-1} Stokes shifts), semiempirical quantum chemical calculations (PM3), and a normal coordinate analysis were used to probe the target molecules $C_{120}O$, $C_{120}O_2$, and $C_{130}O$. $C_{120}O$ and $C_{120}O_2$ were prepared according to literature procedures. $C_{130}O$ was generated (for the first time) in a solid-state reaction between $C_{60}O$ with C_{70}. It was isolated in three isomeric forms. Computational results were also obtained for C_{119} in order to assess to what extent the phenomenology of cage−cage vibrations can be mapped from dimers onto more strongly linked and structurally perturbed "peanuts".

S1089-5639(98)00834-2 CCC: $15.00
Published on Web 05/08/1998

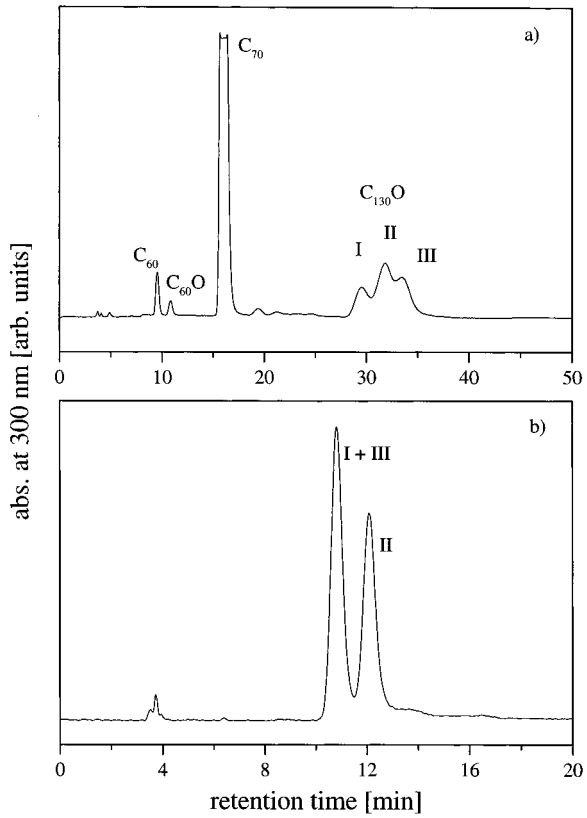

Figure 1. HPLC traces obtained at 300 nm detection upon injecting **I**−**III**) isomer mixture onto (a) semipreparative Cosmosil column (toluene eluent) and (b) Buckyclutcher column (toluene/hexane eluent).

2. Experimental Results

2.1. Preparation. $C_{120}O$ was prepared according to ref 7 by heating a solid mixture of $C_{60}O$ and a roughly 10-fold molar excess of C_{60} to 473 K in a vacuum for 1 h. The microcrystalline reactant mixture was generated by evaporating the solvent from an appropriately partitioned solution (toluene solvent). $C_{120}O_2$ was obtained as a byproduct in the former reaction.[9] $C_{120}O$ and $C_{120}O_2$ were isolated from the microcrystalline product mixture by high-performance liquid chromatography (HPLC) using a Cosmosil Buckyprep column and toluene eluent (one pass). $C_{120}O$ and $C_{120}O_2$ were subsequently studied at purity levels of at least 95%, as determined by a combination of analytical HPLC, matrix-assisted laser desorption time-of-flight mass spectroscopy (MALDI-TOFMS; see below) and Raman measurements.

$C_{130}O$ was synthesized using the same procedure except that a mixture of $C_{60}O$ and a roughly 10-fold molar excess of C_{70} was used. HPLC analysis of the product mixture dissolved in *o*-dichlorobenzene showed three new substances identified as $C_{130}O$ isomers (see below). In order of their elution from the Buckyprep column, we term these isomers of $C_{130}O$ as **I**, **II**, and **III** (see Figure 1). In contrast to $C_{120}O_x$ ($x = 1, 2$), which were isolable via one-stage HPLC fractionation, isolation of **I**−**III** required a three-stage separation protocol. For this, the (solid) product mixture was dissolved in *o*-dichlorobenzene. **I**−**III** were separated from unreacted C_{70}, $C_{60}O$, and C_{60} (reaction byproduct) via a first pass through a Cosmosil Buckyprep column using toluene as eluent. Subsequently, isomers **I** and **III** were separated from isomer **II** using a Regis Buckyclutcher column (eluent consisting of a 3:1 mixture of toluene/hexane). Finally, isomers **I** and **III** were separated from each other by a second pass through the Cosmosil Buckyprep column. Figure 1 illustrates the separation concept by showing typical HPLC traces for the product mixture on a Buckyprep column (step 1 in Figure 1a) followed by an HPLC trace obtained for the $C_{130}O$ (**I**−**III**) isomer mixture on a Buckyclutcher column after removal of C_{60}, $C_{60}O$, and C_{70} (step 2 in Figure 1b). Assuming identical absorption coefficients at 300 nm (HPLC detector), the relative isomer proportion obtained following synthesis and dissolution of the solid product mixture was 3:5:5 for isomers **I**/**II**/**III**. Also, on the basis of this assumption, the $C_{130}O$ isomers subsequently probed were pure to >95%.

$C_{60}O$ was made by reaction of C_{60} with *m*-chloroperoxybenzoic acid according to ref 18. The reaction was periodically checked by HPLC analysis and stopped when $C_{60}O_2$ was detectable. $C_{60}O$ was separated from the product mixture using a Cosmosil Buckyprep column and toluene as eluent. C_{60} and C_{70} were from commercial sources (Hoechst Gold Grade).

The purity of all samples was studied by MALDI-TOFMS. A home-built linear TOF spectrometer (1 m drift tube, 10 kV acceleration voltage) with a multichannel plate ion detector was used.[19] Samples were desorbed from a 9-nitroanthracene matrix using a pulsed N_2 laser (337 nm). Mass resolutions under MALDI conditions for this compound class were >500 at $m/z = 1000$.

Electronic absorption spectra were obtained for all five substances ($C_{120}O$, $C_{120}O_2$ in CS_2 and **I**−**III** in toluene solution). Measurements were performed at room temperature using both a Hitachi U-2000 (2 nm resolution; C_{60}, C_{70}, $C_{120}O$, and **I**−**III**) and a Varian Cary 5E spectrometer (1 nm resolution; $C_{120}O_2$). Resolvable absorption features in the UV−vis spectral region were as follows: $C_{120}O$, 328, 416, 545, and 695 nm; $C_{120}O_2$, 426 nm; **I**, 324 and 397 nm; **II**, 323, 400, 454, and 535 nm; **III**, 323, 403, 448, and 533 nm. On the basis of studies of C_{60} and C_{70}, we expect toluene/CS_2 solution bands for all target molecules to be shifted less than 10 nm relative to corresponding transitions in the solid.[20] We therefore infer from our solution spectra that resonance or preresonance Raman conditions apply to the excitation wavelengths used for studying the corresponding solids (see section 2.2).

2.2. Raman Spectroscopy. Stokes shifted unpolarized Raman spectra were recorded in 180° backscattering geometry using a triple monochromator (Spex TripleMate 1877D) and a CCD camera detector (Photometrics SDS 9000). Excitation light was provided by an Ar^+-pumped titanium sapphire laser (680−850 nm tunability and Ar^+ laser lines). When using the titanium sapphire laser, broad-band laser luminescence was filtered out using a home-built pre-monochromator. Spectra were not corrected for wavelength-dependent detector sensitivity and monochromator throughput (approximately 2× variation over 0−2000 cm^{-1} range for both excitation lines used).

Raman measurements were performed at 514 or 794.76 nm excitation. At 514 nm, the double monochromator of the TripleMate was used as the Rayleigh filter. At 794.76 nm, an alkali vapor cell[21] (K and Rb) with the double monochromator set to zero order was used instead. This wavelength corresponds to the $5^2P_{1/2} \rightarrow 5^2S$ transition in Rb. At resonance, the alkali cell provided higher rejection of Rayleigh light while allowing greater throughput of Raman light than possible with the double monochromator. This is particularly useful for accessing Raman features close to the laser excitation line. For this, the vapor cell was placed between collection optics and the monochromator entrance aperture. Typically, the alkali vapor cell was operated at 473 K and at an N_2 fluorescence quench gas pressure

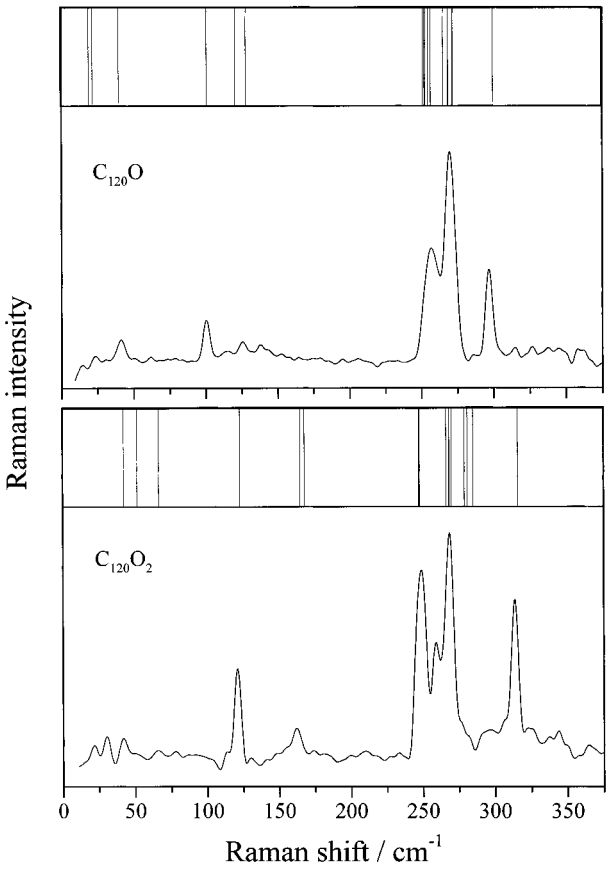

Figure 2. Low-frequency portion of $C_{120}O$ and $C_{120}O_2$ Stokes−Raman spectra (794.76 nm excitation). Spectra were obtained for powdered solids as described in text. Superimposed are PM3 calculations of cage−cage vibrations (15−180 cm^{-1}) and squashing modes (>240 cm^{-1}).

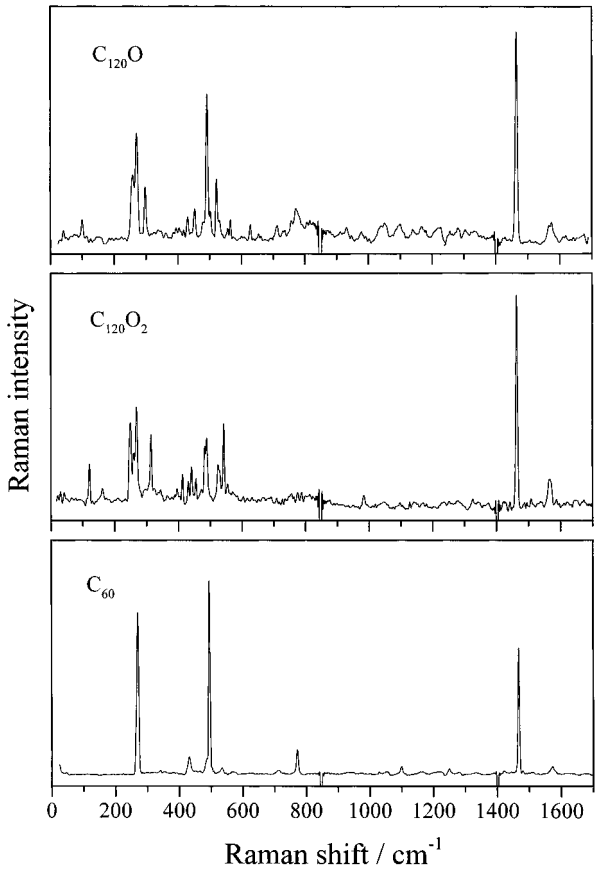

Figure 3. Complete $C_{120}O$ and $C_{120}O_2$ Stokes−Raman spectra (794.76 nm excitation). Also shown is the Raman spectrum of C_{60} obtained at the same excitation wavelength.

of 50 Torr. Under these conditions, the excitation laser (spectral bandwidth of 40 GHz at 794 nm) was attenuated to an OD of 10.

Raman measurements were performed on microcrystalline samples sealed under vacuum in glass or quartz capillaries. Samples were prepared as follows. Solids obtained after eluent evaporation were dispersed/washed in methanol and filtered. The filtrate was again washed with acetone and transferred from the filter to a glass/quartz capillary. This was evacuated to 10^{-2} Torr and sealed under vacuum.

2.2.1. $C_{120}O$ and $C_{120}O_2$ Raman Measurements. $C_{120}O$ and $C_{120}O_2$ Raman spectra (794.76 nm excitation, 200 mW mm^{-2}) extending to within 15 cm^{-1} of the Rayleigh line at an approximate resolution of 2 cm^{-1} were obtained at nominally room temperature. Figure 2 shows the 15−400 cm^{-1} region of these data sets together with PM3 calculations. Figure 3 shows the complete spectra (15−1700 cm^{-1}). Table 1 lists all resolvable Raman features (S/N > 2). For the configuration used, the acquisition of a complete $C_{120}O/C_{120}O_2$ spectrum required the measurement of six adjacent data sets. Each data set required 20 min of data collection time. The spectra shown result from superposition, background subtraction (background = 600% of the most intense Raman feature), and FFT smoothing of the individual data sets. Except for Stokes shifts below 30 cm^{-1} as well as resonances at 848 and 1400 cm^{-1} (Cs impurity in the K/Rb alkali vapor cell), effective background luminescence intensity varied only slightly with frequency.

Although we did not monitor sample temperature during spectral acquisition, there was no evidence of thermal/photochemical degradation of either $C_{120}O$ or $C_{120}O_2$. In particular, we did not observe characteristic (and resolvable—see section 4.6 below) C_{60} features. This is in contrast to preliminary Raman measurements on solid C_{120} at the same excitation wavelength. These show significant (thermal?) degradation to C_{60} upon irradiation.[22]

*2.2.2. Raman Measurements of **I**−**III***. For **I**−**III**, strong luminescence upon excitation in the red prevented measurements with the alkali vapor cell. Therefore, spectra were recorded at 514 nm excitation where luminescence was not as much of a problem (<30% of the most intense Raman feature). As a result, $C_{130}O$ measurements do not extend as close to the Rayleigh line (200−2000 cm^{-1}) as for $C_{120}O/C_{120}O_2$. The spectra comprise three individual data sets obtained at 150 mW mm^{-2} and 4 cm^{-1} resolution. They are shown in Figure 4 after backgound subtraction and FFT smoothing. Table 2 lists all Raman features resolvable for the three isomers. Again, no indication was seen for photochemical/thermal degradation during spectral acquisition.

3. PM3 Calculations

Semiempirical PM3 calculations were performed on an IBM Power PC (RISC 6000: AIX 4.2/128 MB) using the HyperChem software package.[23] As a general rule, approximately 6 weeks of computer time were required for each molecule fully studied (geometry optimization and vibrational frequency analysis).

3.1. Geometries and Ground-State Energetics. Calculations were performed on C_{60}, $C_{60}O$, C_{70}, C_{119}, $C_{120}O$, $C_{120}O_2$, and on five different possible isomers of $C_{130}O$ (**1a**, **1b**, **2**−**4**; see below). For all molecules we started from established/

TABLE 1: $C_{120}O$ and $C_{120}O_2$ Raman Features in cm^{-1}

$C_{120}O$	intensity[a]	$C_{120}O_2$	intensity[a]
41	w	21	w
100	m	31	w
256	s	42	s
269	vs	123	w
297	s	162	s
430	w	248	s
451	w	258	s
491	s	268	s
500	w	313	w
520	m	395	w
550	sh	412	m
557	w	430	m
565	m	441	m
627	m	454	m
654	w	482	m
712	m	488	m
757	m	524	m
770	m	530	m
777	sh	542	m
782	sh	984	m
1051	w	1128	w
1100	w	1464	vs
1140	w	1567	m
1162	w		
1223	w		
1282	w		
1464	vs		
1566	w		
1574	w		

[a] w = weak, m = medium, s = strong, vs = very strong, sh = shoulder.

proposed structures using a molecular mechanics subroutine and performed symmetry-restricted geometry minimizations.

For $C_{120}O$ and $C_{120}O_2$, resulting structures are shown in parts b and c of Figure 5. Geometries and energetics are consistent with previous literature results. Dissociation energies (including zero-point vibration) were calculated as 224 kJ mol^{-1} for $C_{120}O \rightarrow C_{60} + C_{60}O$ and 436 kJ mol^{-1} for $C_{120}O_2 \rightarrow C_{60}O + C_{60}O$. Dissociation barriers were not determined. For C_{119}, we started from the connectivity and symmetry put forward in ref 12 on the basis of ^{13}C NMR measuremements and optimized the structure further. The results are again consistent with literature results. The structure is shown in Figure 5 a.

For $C_{130}O$ we constructed five possible starting geometries based on the assumption that bonding is analogous to $C_{120}O$ (i.e., furanoid ring-bridged). Specifically, the five structures derive from the consideration that every "double" bond in C_{70} is a possible bridging site. In C_{70}, there are four different double bonds. In linking to a double bond in C_{60}, three of these possible bridging sites will form sets of enantiomers, while one bridging site will form a cis/trans isomer depending on the relative orientation of the cages. We label the latter **1a** and **1b**, while the chiral forms are termed **2**−**4**. Figure 6 shows all five optimized structures after energy minimization within the respective symmmetries. Table 3 summarizes their relative energetics. Dissociation energies to $C_{60}O$ and C_{70} were 228, 226, and 228 kJ mol^{-1} for isomers **1a**, **1b**, and **2**, respectively.

3.2. Vibrational Frequencies. For C_{119}, $C_{120}O$, $C_{120}O_2$, **1a**, and **3** vibrational frequencies and infrared intensities were calculated within the harmonic approximation using PM3-optimized structures. Raman cross sections were not determined. We concentrate on the low-frequency region extending to 400 cm^{-1} below.

On the basis of previous PM3 calculations for C_{60} and in particular C_{70}, fullerene vibrational frequencies above 800−1000 cm^{-1} are expected to be accurate to within ±10% after uniform scaling by about 0.85.[24,25] In contrast, for lower frequency modes the best agreement is obtained for unscaled

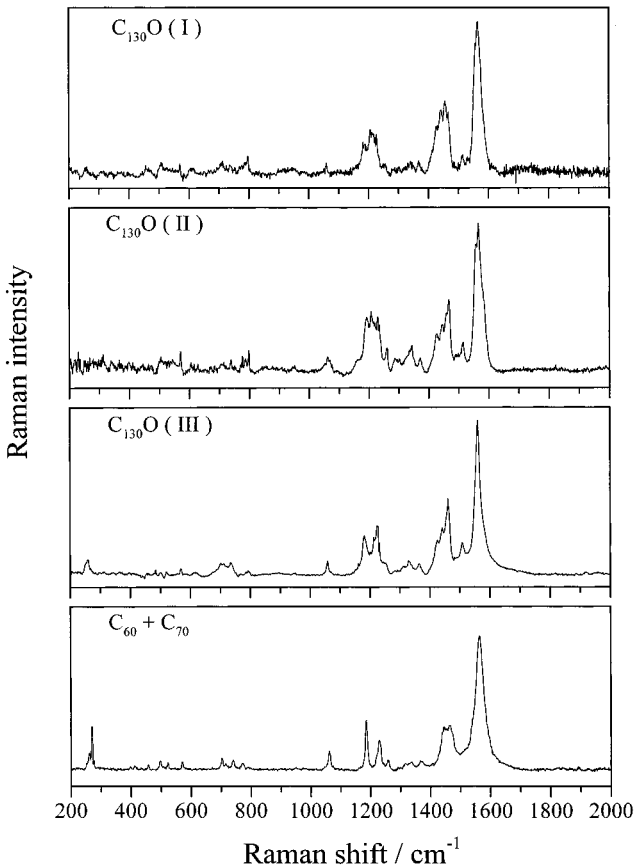

Figure 4. Complete **I**−**III** Stokes−Raman spectra (514 nm excitation). Also shown for comparison is a superposition of C_{60} and C_{70} Raman data sets obtained at the same excitation wavelength. The two data sets were scaled to obtain optimum agreement with $C_{130}O$ results.

TABLE 2: I−III Raman Features in cm^{-1}

I	intensity[a]	**II**	intensity[a]	**III**	intensity[a]
454	w	570	w	257	m
506	w	604	w	484	w
569	w	627	w	567	w
709	w	737	w	702	w
796	w	776	w	710	w
1058	w	787	w	721	w
1187	m	797	w	734	w
1205	m	950	w	786	w
1214	m	1052	w	795	w
1226	m	1062	m	1058	m
1248	w	1068	m	1180	m
1256	w	1193	m	1201	m
1331	w	1208	m	1212	m
1339	w	1219	m	1222	m
1367	w	1229	m	1233	m
1427	m	1235	m	1330	w
1442	m	1259	m	1364	w
1456	m	1302	m	1425	s
1466	m	1342	m	1441	s
1513	m	1370	m	1460	s
1565	s	1426	m	1509	m
		1444	m	1561	s
		1466	s		
		1512	w		
		1556	s		
		1566	s		

[a] w = weak, m = medium, s = strong, vs = very strong, sh = shoulder.

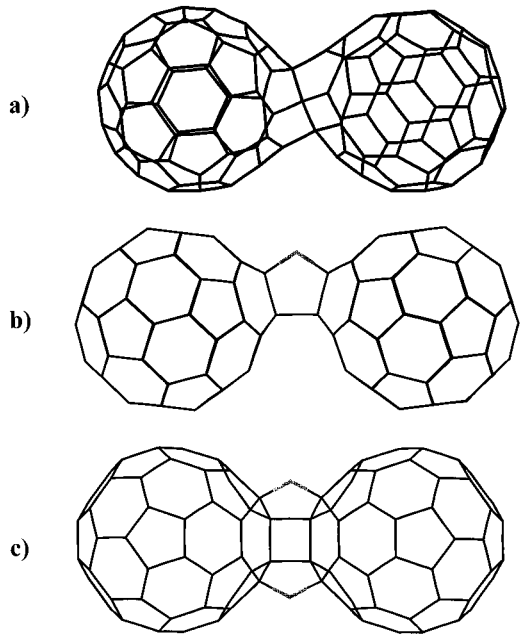

Figure 5. PM3-optimized geometries for the accepted electronic ground states of C_{119} (a), $C_{120}O$ (b), and $C_{120}O_2$ (c). See text for details.

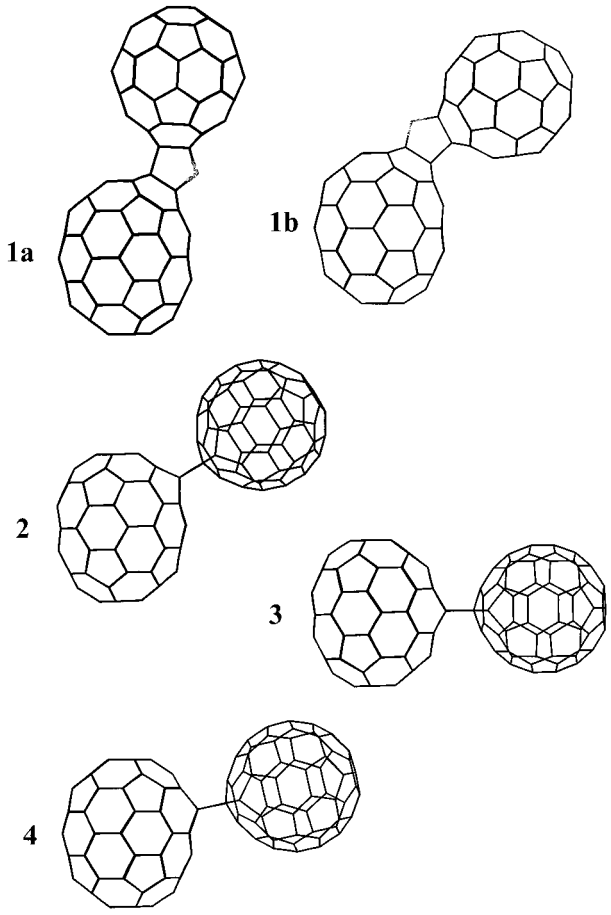

Figure 6. PM3-optimized geometries for the five possible $C_{130}O$ isomers (**1a**, **1b**, **2**−**4**) resulting from hypothetical 1,2-addition of $C_{60}O$ to C_{70}.

calculations.[25] It is not immediately obvious why this should be the case, although lower frequency vibrations are presumably more strongly affected by matrix shifts. For all five molecules, Table 4 lists unscaled vibrational frequencies found to lie within 0−400 cm^{-1}.

TABLE 3: PM3 Calculations of Electronic Ground States

species	symmetry	total energy/au[a]
C_{119}	C_2	−516.311 329
$C_{120}O$	C_{2v}	−531.455 375
$C_{120}O_2$	C_{2v}	−542.295 931
1a	C_s	−574.940 566
1b	C_s	−574.940 749
2	C_1	−574.941 453
3	C_s	−574.861 465
4	C_1	−574.929 415

[a] 1 au = 2625 kJ mol^{-1}.

4. Discussion

4.1. Systematics of Cage−Cage Modes. The superposition of experimental and computational results shown in Figure 2 for $C_{120}O$ and $C_{120}O_2$ indicates that their low-frequency Raman features may be divided into two regions: 15−180 and 240−375 cm^{-1}. A computer visualization of the corresponding normal mode motion for the (gas-phase) dimers shows that the 15−180 cm^{-1} region comprises exclusively cage−cage vibrations. These are defined as torsions or stretches of the hollow carbon cluster masses relative to each other (with some oxygen atom contributions but little intracage motion). For both molecules there are six such modes. They are followed to higher energy by cage deformation modes (e.g., squashing) interspersed with furan ring vibrations (200−400 cm^{-1}). Beyond this energy range other types of vibration set in, encompassing increasing amounts of tangential intracage atom motion. Our analysis suggests that this systemization is also applicable to $C_{130}O$ and C_{119}.

Figure 7 provides a visualization of all cage−cage modes calculated for $C_{120}O$. These comprise five cage−cage torsional modes (ν_1−ν_3, ν_5, and ν_6) as well as what is essentially a symmetric stretch vibration (ν_4) analogous to that of a diatomic molecule ("superdiatomic" mode). The six lowest frequency vibrations of C_{119}, $C_{120}O_2$, **1b**, and **3** are calculated to be strictly analogous in terms of their motions and energy ordering.

The occurrence of six well-defined low-frequency cage−cage modes implies that these fullerene dimers may be idealized as rigid hollow spheres connected by two (short) equivalent bonds that define a bonding plane. Without these bonds, each sphere has three (degenerate) rotational and three translational degrees of freedom, 12 altogether. Linking the spheres (in a bonding plane) reduces the translational and rotational degrees of freedom to three and three, respectively. There should consequently be $12 - 6 = 6$ remaining mechanical degrees of freedom. Group theory (D_{2h}) shows that these degrees of freedom must comprise exactly five torsional modes (coupled rotations) and one symmetric stretch vibration (coupled translations). The corresponding motions are represented schematically in Figure 8. An analogous picture applies to any two coupled rigid rotors of lower symmetry. We note in passing that a "superdiatomic" molecule has *three* rotational degrees of freedom (including a rotation about the "bond" axis) versus two for a classical diatomic molecule composed of point masses.

4.2. $C_{120}O$ and $C_{120}O_2$ Spectral Assignment. Figure 2 demonstrates good agreement between results from the PM3 calculation and experiment for $C_{120}O$ and $C_{120}O_2$ in the 15−400 cm^{-1} region. Note that both $C_{120}O$ and $C_{120}O_2$ have C_{2v} symmetry. Consequently, all possible vibrations are Raman active ($C_{120}O$, $92A_1 + 82A_2 + 91B_1 + 87\ B_2$; $C_{120}O_2$, $93A_1 + 88A_2 + 91B_1 + 88B_2$). Accuracy over the 0−400 cm^{-1} range is expected to be equally good for the other species calculated in this study (excepting perhaps C_{119} in which a somewhat

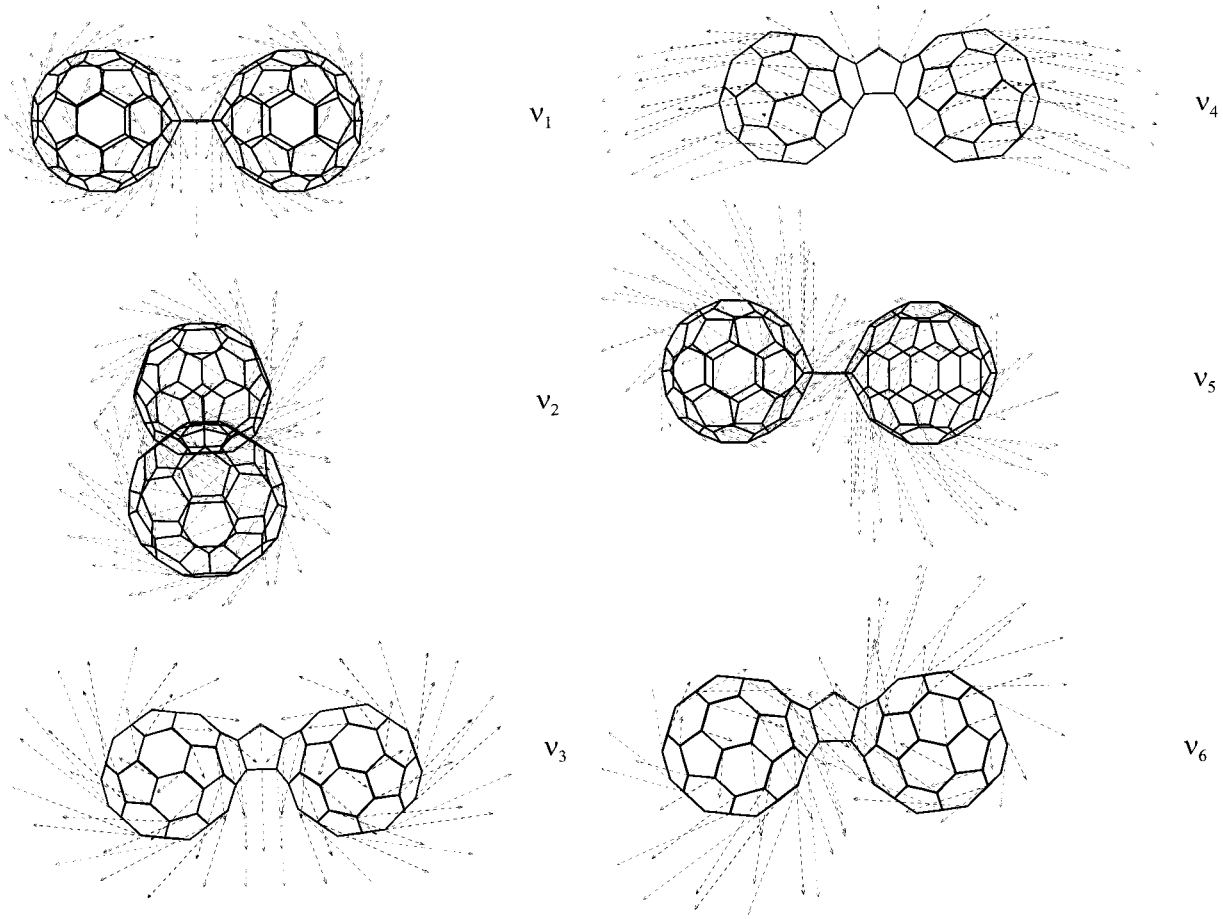

Figure 7. Parts a (left-hand side) and b (right-hand side) show a visualization of the six lowest energy vibrational modes of $C_{120}O$. All are Raman allowed.

TABLE 4: PM3 Calculations of Low-Frequency Vibrations (0−320 cm^{-1}) of C_{119}, $C_{120}O$, $C_{120}O_2$, 1a, and 3

C_{119}	symmetry	$C_{120}O_2$	symmetry	$C_{120}O$	symmetry	**1a**	symmetry	**3**	symmetry
44	A	42	A_1	19	B_1	18	A″	20	A″
52	A	52	A_2	22	A_2	21	A″	22	A″
62	B	67	B_1	40	A_1	37	A′	38	A′
119	A	123	A_1	101	A_1	94	A′	94	A′
169	A	165	A_2	121	A_2	116	A″	115	A″
184	B	168	B_2	128	B_2	124	A′	119	A′
231	A	247	B_2	251	B_1	216	A″	226	A′
235	B	248	A_1	252	A_2	218	A′	228	A′
239	B	248	A_2	253	B_2	250	A″	234	A″
240	A	248	B_1	255	A_1	252	A″	249	A″
273	B	266	B_2	257	B_1	253	A′	252	A′
275	B	268	B_2	266	B_2	254	A″	254	A″
275	A	268	A_2	269	B_2	255	A′	255	A″
278	A	270	A_1	269	A_2	263	A′	256	A′
280	B	279	B_1	272	B_1	270	A′	270	A′
313	A	281	A_1	272	A_1	270	A″	271	A″
		285	B_1	300	A_1	291	A′	287	A′
		316	A_1						

different bonding situation pertains). Section 4.3 is based on this assumption.

We concentrate on the low-frequency cage−cage vibration range (15−180 cm^{-1}). As listed in Table 1, Raman features were clearly resolved at 41 and 100 cm^{-1} for $C_{120}O$ and 21, 31, 42, 123, and 162 cm^{-1} for $C_{120}O_2$. Note that the $C_{120}O$ and $C_{120}O_2$ Raman spectra recently obtained at 1064 nm excitation are fully consistent with our measurements but do not extend as close to the Rayleigh line.[17] Consequently, the $C_{120}O$ feature at 41 and $C_{120}O$ features at 21, 31, and 42 cm^{-1} were not previously observed. Using our PM3 predictions, we tentatively assign the observed Raman bands as follows: $C_{120}O$ (symmetry/expt/PM3), ν_3 (A_1/41/40 cm^{-1}), ν_4 (A_1/100/101 cm^{-1}); $C_{120}O_2$ (symmetry/expt/PM3), ν_1 (A_1/21/42 cm^{-1}), ν_2 (A_2/31/52 cm^{-1}), ν_3 (B_2/42/67 cm^{-1}), ν_4 (A_1/123/123 cm^{-1}), and ν_5 (A_2/162/165 cm^{-1}). On this basis, the 15−60 cm^{-1} spectral range, in particular of $C_{120}O_2$, seems less satisfactorily described than the higher frequency cage−cage vibrations, which are in almost quantitative agreement with experimental results . This may reflect idiosyncracies of the PM3 parametrization in describing $C_nO_2C_n$ vs C_nOC_n links.

Alternatively, these discrepancies may reflect condensed-phase phenomena such as matrix shifts, *intramolecular* librations, or indeed coupled inter- and intramolecular librational

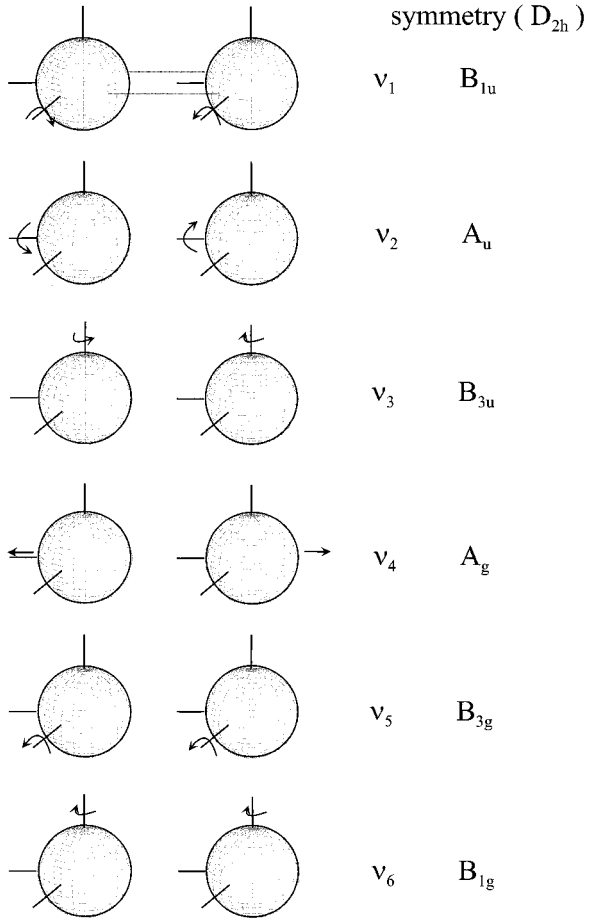

Figure 8. Idealized model of the six superdiatomic vibrations assuming three rotational and three translational degrees of freedom for each hollow sphere before coupling.

motion. Intramolecular librations have been well studied for C_{60},[26] where they become important/resolvable at temperatures below the fcc → sc transition.[26] At 77 K, the integrated librational mode intensity was found to be about $^1/_{150}$ of the most intense C_{60} Raman feature ($A_g(1)$, 496 cm^{-1}). Should it be possible to obtain well-defined crystalline samples of $C_{120}O$ and $C_{120}O_2$, it will be informative to carry out Raman measurements at lower temperatures to pursue this issue further. These measurements would be usefully complemented by ab initio calculations of nonresonant Raman cross sections.[22]

4.3. Superdiatomic Mode. Of particular interest in both $C_{120}O$ and $C_{120}O_2$ Raman spectra are the superdiatomic symmetric stretch ν_4 modes (both A_1 symmetry) occurring/calculated at 100/101 and 123/123 cm^{-1}, respectively. For the **1a** and **3** isomers of $C_{130}O$, the analogous vibration is calculated to occur at 93 and 94 cm^{-1}, respectively. C_{119} is calculated to have such a mode at 116 cm^{-1}, consistent with previous predictions.[27] On the basis of these five examples of short-linked fullerene dimers containing C_{60} and C_{70}, the (always Raman active) superdiatomic mode consistently occurs in the frequency interval of 90−120 cm^{-1}.

C_{120} Raman spectra obtained by Lebedkin et al. show three features in the 90−180 cm^{-1} region: a moderately strong peak at 96 cm^{-1} and two weak features at 127 and 139 cm^{-1}.[17] The 96 cm^{-1} peak can be definitively assigned to the superdiatomic vibration as follows. C_{120} has D_{2h} symmetry.[6] Consequently, the molecule can have A_g, A_u, B_{1g}, B_{2g}, B_{3g}, B_{1u}, B_{2u}, and B_{3u} symmetry vibrations. Only gerade modes are Raman active. We expect the six low-frequency cage−cage vibrations again

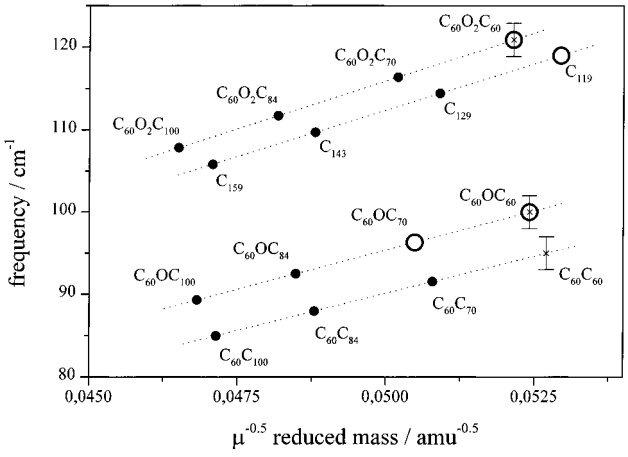

Figure 9. Summary of existing superdiatomic symmetric stretch data/calculation as well as first-order prediction for as yet uncharacterized species. Plotted are the symmetric stretch frequency versus the fullerene dimer reduced mass (see text). We distinguish between four C_{60}-derived dimer types: bis(furanoid) link, "peanut", furanoid link, and 2 + 2 cycloadduct. Experimental data are shown for C_{120} (×, ref 17), $C_{120}O$, and $C_{120}O_2$ (×, this work). PM3 calculations are plotted for C_{119}, $C_{120}O$, $C_{120}O_2$, **1a**, **1b**, and **3** (○, this work). The other points correspond to prediction for various heterodimers based on the assumption that the force constants corresponding to each dimer type are independent of which fullerene is attached to the common unit.

to be well separated from the intracage region (see section 4.1 above). Furthermore, these cage−cage modes should be analogous to and have the same general energy ordering as found for $C_{120}O$ and $C_{120}O_2$. Imposing the higher symmetry of C_{120} ($C_{2v} \rightarrow D_{2h}$), we expect B_{1u}, A_u, B_{3u}, A_g, B_{3g}, and B_{1g} modes in order of increasing energy (see Figure 8). Consequently, only three of these cage−cage vibrations should be observable of which the lowest energy is the superdiatomic ν_4-(A_g) mode at 96 cm^{-1}. Note further that $\nu_1(B_{1u})$ and $\nu_3(B_{3u})$ are IR active while $\nu_2(A_u)$ is silent.

4.4. Picosprings and Isotopic Substitution. Figure 9 contains a summary of available superdiatomic mode frequencies grouped according to compound class: bis(furanoid) ring link, furanoid ring link, cyclobutane link, and "peanut". Plotted, versus reduced mass, are our PM3 frequencies and/or experimental data . We have also included the C_{120} measurement of ref 17. Reduced masses were calculated for the assumed mass distributions of $C_{60}-C_x$, $C_{60}O-C_x$, $C_{60}O_2-C_x$, and $C_{61}-C_x$.

Using Hook's law ($\omega = (k/\mu)^{1/2}$), one can determine harmonic force constants for the respective links. For 2 × C_{60}-derived dimers, we find the following k ordering: $C_{120} < C_{120}O < C_{119}$, $C_{120}O_2$. Interestingly, this k ordering corresponds inversely to the degree of parent ion fragmentation observed in laser desorption time-of-flight mass spectroscopy (see above).

Can one take the analogy one step further, with heterodimers (e.g., $C_{130}O$) as isotopically substituted homodimers? The superdiatomic frequencies computed for **1a** and **3** yield almost exactly the same force constants as determined for $C_{120}O$. Figure 9 therefore also contains entries for several as yet unknown high fullerene/C_{60} combinations under the assumption that the respective (harmonic) force constants remain constant for the same link-type, independent of heterofullerene appendage (mass). Lines are based on PM3 k values calculated for the respective homodimers. Note that the resulting lines extrapolate to the vibrational frequency of a C_{60} unit appropriately linked to an infinite graphite sheet (corresponding to $\mu^{-1/2} = 0.037$ $amu^{-1/2}$).

4.5. $C_{130}O$: Which Isomers Are Formed? Figure 4 indicates that **I**−**III** have very similar Raman features, with

minor variations apparent in particular near 1200 cm^{-1}. This is consistent with our calculations on **1a** and **3**, which suggest that both inter- and intracage vibrational frequencies are not strongly dependent on isomer form.[22] For example, Table 4 indicates differences of generally 1−2 cm^{-1} (and at most 16 cm^{-1}) between corresponding vibrations in **1a** and **3**. Given the measurement *S*/*N*, we have not attempted to determine the isomers formed on the basis of their Raman spectra.

On the basis of their calculated total energies (Table 3), isomers **1a**, **1b**, and **2** are significantly favored over **3** and **4**. Free energies at 473 K were not determined. However, we do not expect the ordering to be significantly different given the uniformly weak intracage vibrational coupling. Fowler et al. have performed MNDO calculations on **1a**, **1b**, and **2**, arriving at relative total energies of 0.0, 0.4, and 3.6 kJ/mol, respectively.[28] Although the exact energy ordering is not the same as in our PM3 calculations, the inference that these three isomers should be the most stable (of five) is the same. Note that MNDO, AM1, and PM3 semiempirical parametrizations as applied to fullerenes and related structures in this size range can differ in relative energy prediction by ±5 kJ/mol.[28] Consequently, the lowest energy form of $C_{130}O$ cannot be determined at the semiempirical level. By now there is also an extensive synthetic database on which to base expectation for the isomers formed by nucleophilic 1,2-addition to C_{70}. Predominantly C(1)−C(2) and C(5)−C(6) adducts are observed, corresponding to addition in regions of highest cage curvature.[29] In our nomenclature, the former corresponds to **1a** and **1b** while the latter gives rise to **2**. Consequently, it is likely that **1a**, **1b**, and **2** have been generated in this study. Given that the Raman spectra of **I** and **II** appear similarly broadened while that of **III** is somewhat sharper, we tentatively assign **I**/**II** to structures **1a**/**1b**, while **III** may correspond to **2**. The electronic absorption spectra obtained for **I** and **II** versus **III** are not inconsistent with this assignment.

As yet, we do not have enough material to attempt ^{13}C NMR measurements. A clear structural determination must therefore await further work.

4.6. $C_{130}O$ Raman as a Superposition of C_{60} and C_{70}. In Figure 4 we have attempted to describe the **I**−**III** Raman spectra as a linear superposition of C_{60} and C_{70} measurements obtained at 514 nm. C_{60} and C_{70} spectra were arbitrarily scaled to obtain the best agreement to $C_{130}O$. The level of agreement is good. The most obvious discrepancies between superposition and $C_{130}O$ measurement are (i) a systematic blue shift of up to 5 cm^{-1}, (ii) no symmetry splitting, and (iii) the absence of cage−cage and furanoid ring modes. Effect i is likely due to relaxation of cage regions adjacent to the link, thus inducing a red shift of intracage modes. Neglecting resonance coupling[30] and the possibility of charge-transfer excitations, the optimized superposition allows a rough assessment of overall Stokes−Raman cross section ratios for C_{60} versus C_{70} at 514 nm excitation. The real contributions of C_{60} and C_{70} data sets to the integrated superposition shown in Figure 6 are about 1:2.

5. Summary

Several examples of chemically linked fullerene dimers with short cage−cage separations are now known. In this study we have been interested in their characteristic vibrational properties. For this purpose we have prepared $C_{120}O$, $C_{120}O_2$, and three isomers of $C_{130}O$ (**1a**, **1b**, and **2**). The latter correspond to the first fullerene heterodimers yet isolated.

These dimers were studied both experimentally (Raman measurements of $C_{120}O$, $C_{120}O_2$, and $C_{130}O$) and computationally (ground-state energetics and vibrational frequencies at the PM3 level) with particular emphasis on low-frequency cage−cage vibrations. There are always six such vibrations in the 15−180 cm^{-1} region, one of which corresponds to the Raman allowed symmetric stretch mode, much like the vibration of a diatomic molecule. This vibration as well as the other five (torsional) modes can be understood in terms of the motional degrees of freedom of a weakly coupled "superdiatomic" comprised of near-rigid hollow spheres. Such compounds or derivatives thereof may be of further interest for systematic studies of vibrational energy flow and perhaps funneling in large molecules.[31]

Acknowledgment. This work was supported by the Deutsche Forschungsgemeinschaft under Sonderforschungsbereich 551 "Kohlenstoff aus der Gasphase: Elementarreaktionen, Strukturen, Werkstoffe". We thank S. Lebedkin for communication of C_{120}, $C_{120}O$, and $C_{120}O_2$ Raman results prior to publication.

References and Notes

(1) Yeretzian, C.; Hansen, K.; Diederich, F.; Whetten, R. *Nature* **1992**, *359*, 44.

(2) Rao, A.; Zhou, P.; Wang, K.-A.; Hager, G.; Holden, J.; Wang, Y.; Lee, W.-T.; Bi, X.-X.; Ecklund, P.; Cornett, D.; Duncan, M.; Amster, I. *Science* **1993**, *259*, 955. Zhou, P.; Dong, Z.-H.; Rao, A.; Ecklund, P. *Chem. Phys. Lett.* **1993**, *211*, 337.

(3) See, for example, the following. *Appl. Phys. A* **1997**, *64* (3). Goze, C.; Rachdi, F.; Hajji, L.; Nunez-Regueiro, M.; Marques, L.; Hodeau, J.-L.; Mehring, M. *Phys. Rev. B* **1996**, *54*, 3676 and references therein.

(4) See, for example, the following. Thier, K.-F. Mehring, M.; Rachdi, F. *Phys. Rev. B* **1996**, *55*, R496 references therein.

(5) See, for example, the following. Rubin, Y. In *The Chemical Physics of Fullerenes 10 (and 5) Years Later: The Far-Reaching Impact of the Discovery of C_{60}*; Andreoni, W., Ed.; Kluwer Academic: Dordrecht, 1996.

(6) Wang, G.-W.; Komatsu, K.; Murata, Y.; Shiro, M. *Nature* **1997**, *387*, 583.

(7) Lebedkin, S.; Ballenweg, S.; Gross, J.; Taylor, R.; Krätschmer, W. *Tetrahedron Lett.* **1995**, *36*, 4971.

(8) Smith, A., III; Tokuyama, H.; Strongin, R.; Furst, G.; Romanow, W. *J. Am. Chem. Soc.* **1995**, *117*, 9359.

(9) Gromov, A.; Lebedkin, S.; Ballenweg, S.; Avent, A.; Taylor, R.; Krätschmer, W. *Chem. Commun*. **1997**, 209.

(10) McElvany, S.; Callahan, J.; Ross, M.; Lamb, L.; Huffman, D. *Science* **1993**, *260*, 1632.

(11) Beck, R.; Bräuchle, G.; Stoermer, C.; Kappes, M. *J. Chem. Phys.* **1995**, *102*, 540.

(12) Gromov, A.; Ballenweg, S.; Giesa, S.; Lebedkin, S.; Hull, W.; Krätschmer, W. *Chem. Phys. Lett*. **1997**, *267*, 460.

(13) Adams, G.; Page, J.; Sankey, O.; O'Keeffe, M. *Phys. Rev. B* **1994**, *50*, 17471.

(14) Porezag, D.; Pederson, M.; Frauenheim, T.; Köhler, T. *Phys. Rev. B* **1995**, *52*, 14693.

(15) Pederson, M.; Quong, A. *Phys. Rev. Lett*. **1995**, *74*, 2319.

(16) Porezag, D.; Jungnickel, G.; Frauenheim, T.; Seifert, G.; Ayuela, A.; Pederson, M. *Appl. Phys. A* **1997**, *64*, 321.

(17) Lebedkin, S.; Gromov, A.; Giesa, S.; Gleiter, R.; Renker, B.; Rietschel, H.; Krätschmer, W. *Chem. Phys. Lett.* **1998**, *285*, 210.

(18) Balch, A.; Costa, D.; Noll, B.; Olmstead, M. *J. Am. Chem. Soc*. **1993**, *117*, 8926.

(19) Stoermer, C.; Gilb, S.; Friedrich, J.; Schooss, D.; Kappes, M. *Rev. Sci. Instrum*., in press.

(20) See, for example, the following. Renge, I. *J. Phys. Chem*. **1995**, *99*, 13830.

(21) See, for example, the following. Pelletier, M. *Appl. Spectrosc*. **1993**, *47*, 69 and references therein.

(22) Eisler, H.-J.; Hennrich, F.; Kappes, M. In *Molecular Nanostructures, Proceedings Int. Wintesschool on Electronic Properties of Novel Materials*; Roth, S., Mehring, M., Fink, J., Kuzmany, H., Eds.; World Scientific: Singapore, 1998.

(23) *HYPERCHEM*, Version 4.5 (program including backend for UNIX); Hypercube Inc.: Waterloo, Canada, 1995.

(24) See, for example, the following. Bakowies, D.; Thiel, W. *Chem. Phys*. **1991**, *151*, 309.

(25) Brockner, W.; Menzel, F. *J. Mol. Struct*. **1996**, *378*, 147.

(26) Horoyski, P.; Thewalt, M. *Phys. Rev. B* **1993**, *48*, 11446. Wolk, J.; Horoyski, P.; Thewalt, M. *Phys. Rev. Lett*. **1995**, *74*, 3483. Horoyski,

P.; Thewalt, M.; Anthony, T. *Phys. Rev. B* **1995**, *52*, R6951. Horoyski, P.; Thewalt, M. *Phys. Rev. B* **1996**, *53*, 2199.

(27) Adams, G.; Page, J.; O'Keeffe, M.; Sankey, O. *Chem. Phys. Lett*. **1994**, *228*, 485.

(28) Fowler, P.; Mitchell, D.; Taylor, R.; Seifert, G. *J. Chem. Soc., Perkin Trans. 2* **1997**, 1901.

(29) Thilgen, C.; Herrmann, A.; Diederich, F. *Angew. Chem.* **1997**, *109*, 2362.

(30) Gallagher, S.; Armstrong, R.; Clucas, W.; Lay, P.; Reed, C. *J. Phys. Chem. A* **1997**, *101*, 2960. Gallagher, S.; Armstrong, R.; Bolskar, R.; Lay, P.; Reed, C. *J. Am. Chem. Soc*. **1997**, *119*, 4263.

(31) Jiang, D.-L.; Aida, T. *Nature* **1997**, *388*, 454.